Available online at www.sciencedirect.com
SCIENCE DIRECT®
International Journal of Heat and Fluid Flow 26 (2005) 133–140
International Journal of HEAT AND FLUID FLOW
www.elsevier.com/locate/ijhff

Experimental and theoretical study of the interfacial instability between two shear fluids in a channel Couette flow

Lichun Dong, Duane Johnson *

Department of Chemical Engineering, University of Alabama, A 127 Bevill Building, Box 870203, Tuscaloosa, AL 35487-0203, USA

Received 13 October 2003; accepted 4 April 2004
Available online 7 June 2004

Abstract

The instabilities of a channel Couette flow composed of two layers of immiscible fluids were investigated experimentally and compared with the theoretical predictions of a linear instability analysis. The results show that in the shortwave instability regime, the experimental results agree well with the theoretical predictions of the linear instability analysis. However, we can find shortwaves even in the range of the depth ratios when the linear instability predicts only longwaves are unstable. The reasons are believed to be the dimensional limitation of the experimental apparatus and the existence of the outside and inside wall. In addition, we studied the dependence of the onset of the shortwaves on the viscosity and density of the fluids.

Keywords: Linear instability; Channel Couette flow; Two-layer flow; Shortwaves

1. Introduction

Interfacial instabilities in multiple fluid layers has received much attention for their importance in engineering processes, such as coatings, polymer extrusion, oil transportation, as well as their basic scientific significance. Linear stability analyses have identified three types of instabilities: a long-wavelength instability (Yih, 1967), a short-wavelength instability (Hooper and Boyd, 1983) and an intermediate-wavelength instability whose wavelength is of the order of the thickness of the fluid layer (Renardy, 1985). However, even with the huge amount of literature on the linear instability of the two-phase flow, few papers (Renardy, 1985; Gallagher et al., 1996; Kuru et al., 1985) solved the problem for arbitrary wavenumber, showed the instability regime and investigated the influence of the physical properties on the critical Reynolds number. Moreover, liquid–liquid experiments of the two-phase flow are even less common (Gallagher et al., 1996; Kao and Park, 1972; Sangalli et al., 1995).

Gallagher et al. (1996) investigated the interfacial instability caused by viscosity stratification of a density-matched, two-layer, rotating Couette flow. Their results showed that depending on the depth ratio of the system, the stability of the interface varies greatly. If longwaves are unstable, interfacial waves do not appear at a rotation speed that seems to be related to linear instability analysis and the waves that appear, are not usually very periodic. Thus at these conditions, the linear theory does not match the experimental results. When the less viscous fluid is sufficiently thin, the system is stable to longwaves (a typical behavior for stratified flows) but can be unstable to shortwaves. In this region, the experimental results are close to linear predictions.

In this paper we studied the instabilities of two superposed viscous layers in a channel Couette flow and compared the theoretical predictions of linear instability analysis with our experimental data. Our results show that in the shortwave instability regime, our experimental data agree well with the predictions of the linear instability analysis. However, in the longwave instability regime where linear instability analysis predicts that shortwaves are stable, we also find the shortwave instability in our experiments. Furthermore, the influence of the viscosity and density of the two liquids on

* Corresponding author. Tel.: +1-205-348-8402; fax: +1-205-348-7558.
E-mail address: djohnson@coe.eng.ua.edu (D. Johnson).

0142-727X/$ - see front matter © 2004 Elsevier Inc. All rights reserved.
doi:10.1016/j.ijheatfluidflow.2004.04.001

Nomenclature

Re	critical Reynolds number based on the bottom layer	σ_0	the interfacial tension between two fluids
Re^+	critical Reynolds number based on the upper layer	k	the dimensionless wavenumber
l	depth ratio	λ	the wavelength
r	density ratio	d^+, d	the thickness of the top and bottom fluids, respectively
m	viscosity ratio	ρ^+, ρ	the density of the top and bottom fluids, respectively
C	the Capillary number	μ^+, μ	the viscosity of the top and bottom fluids, respectively
G	the Grashof number		

the stability of the flow in the shortwave instability regime was also studied.

2. Theory

2.1. Governing equation and boundary condition

Two fluids of different viscosity (μ^+, μ), kinematic viscosity (v^+, v), and density (ρ^+, ρ) lie between two rigid parallel boundaries of semi-infinite extent in the (x^*, z^*) plane (Fig. 1). The physical properties of the fluid with superscript + denote the upper layer. The lower layer occupies $-d \leqslant z \leqslant 0$ and the upper layer occupies $0 \leqslant z^* \leqslant d^+$. Asterisks denote dimensional variables. The lower boundary at $z = -d$ moves with velocity U_0 and the upper boundary is fixed. The fluids are incompressible and satisfy the Navier–Stokes equation. At the interface, the velocity and shear stress must be continuous, the jump in the normal stress is balanced by surface tension and surface curvature, and the kinematic free surface condition must hold. We introduce the following dimensionless variables (without asterisks).

$$(x, z) = (x^*, z^*)/d, \qquad t = t^* v/(d)^2, \qquad \mathbf{v} = \mathbf{v}^* d/v,$$
$$p = p^*(d)^2/\mu v$$

where $\mathbf{v} = (u, w)$ is the velocity vector, and p is the pressure.

After the non-dimensionalization, the governing equations of motion and boundary conditions become:

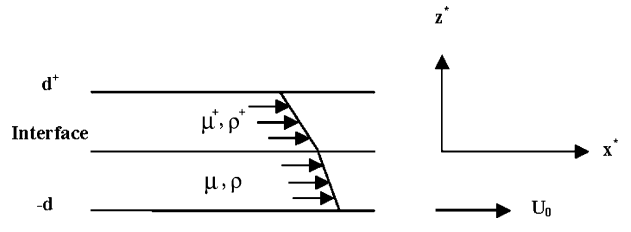

Fig. 1. The flow configuration of undisturbed two-layer Couette flow. The lower layer fluid occupies $-d \leqslant z^* \leqslant 0$ and the upper layer fluid occupies $0 \leqslant z^* \leqslant d^+$.

For the upper fluid (fluid 2):

$$\nabla \cdot \mathbf{v}^+ = 0 \tag{1}$$

$$\frac{\partial \mathbf{v}^+}{\partial t} + \mathbf{v}^+ \cdot \nabla \mathbf{v}^+ = r^{-1}(-\nabla p^+ + m\nabla^2 \mathbf{v}^+) \tag{2}$$

For the bottom fluid (fluid 1):

$$\nabla \cdot \mathbf{v} = 0 \tag{3}$$

$$\frac{\partial \mathbf{v}}{\partial t} + \mathbf{v} \cdot \nabla \mathbf{v} = -\nabla p + \nabla^2 \mathbf{v} \tag{4}$$

where $r = \rho^+/\rho$ is the density ratio, $m = \mu^+/\mu$ is the viscosity ratio.

The eight boundary conditions used to solve the equations are continuity of velocity parallel and normal to the walls,

$$u^+ = w^+ = 0 \quad \text{at } z = l \tag{5}$$

$$u = Re, \quad w = 0 \quad \text{at } z = -1 \tag{6}$$

where $l = d^+/d$ is the depth ratio, and $Re = dU_0/v$ is the Reynolds number based on the bottom layer parameters. Continuity of velocity at the interface $z = \zeta(x, t)$ gives

$$u^+ = u \tag{7}$$

$$w^+ = w \tag{8}$$

Continuity of normal and tangential stress at the interface gives

$$\mathbf{n} \cdot m[\nabla \mathbf{v}^+ + (\nabla \mathbf{v})^{\mathrm{T}}] \cdot \mathbf{n} - p^+ = \mathbf{n} \cdot [\nabla \mathbf{v} + (\nabla \mathbf{v})^{\mathrm{T}}] \cdot \mathbf{n} - p + G\mathbf{z} + C^{-1}\nabla \cdot \mathbf{n} \tag{9}$$

$$\mathbf{t} \cdot m[\nabla \mathbf{v}^+ + (\nabla \mathbf{v}^+)^{\mathrm{T}}] \cdot \mathbf{n} = \mathbf{t} \cdot [\nabla \mathbf{v} + (\nabla \mathbf{v})^{\mathrm{T}}] \cdot \mathbf{n} \tag{10}$$

where $C = \sigma_0 d/(\mu v)$ is the Capillary number, and $G = (\rho - \rho^+)gd^3/(\mu v)$ is the Grashof number. $\mathbf{n}$ is the unit normal vector, $\mathbf{t}$ is the unit tangential vector, σ_0 is the interfacial tension between two fluids.

Additionally, a kinematic boundary condition is required for dynamic surface deformations.

$$u^+ = \frac{\mathrm{d}\zeta}{\mathrm{d}t} \tag{11}$$

2.2. Linear stability analysis

The stability of this flow is examined using a standard linear stability analysis, where the dependent variables are expanded about some parameter, ε.

$$(u^+, w^+, p^+, u, w, p)^t = (u_0^+, w_0^+, p_0^+, u_0, w_0, p_0)^t + \varepsilon(u_1^+, w_1^+, p_1^+, u_1, w_1, p_1)^t + \mathrm{O}(\varepsilon^2) \tag{12}$$

At the interface:

$$u^+ = u_0^+ + \varepsilon u_1^+ + \varepsilon \frac{\partial u_0^+}{\partial z}\zeta_1 + \mathrm{O}(\varepsilon^2) \tag{13}$$

$$w^+ = w_0^+ + \varepsilon w_1^+ + \varepsilon \frac{\partial w_0^+}{\partial z}\zeta_1 + \mathrm{O}(\varepsilon^2) = \varepsilon w_1^+ + \mathrm{O}(\varepsilon^2) \tag{14}$$

$$p^+ = p_0^+ + \varepsilon p_1^+ + \varepsilon \frac{\partial p_0^+}{\partial z}\zeta_1 + \mathrm{O}(\varepsilon^2) = p_0^+ + \varepsilon p_1^+ + \mathrm{O}(\varepsilon^2) \tag{15}$$

$$u = u_0 + \varepsilon u_1 + \varepsilon \frac{\partial u_0}{\partial z}\zeta_1 + \mathrm{O}(\varepsilon^2) \tag{16}$$

$$w = w_0 + \varepsilon w_1 + \varepsilon \frac{\partial w_0}{\partial z}\zeta_1 + \mathrm{O}(\varepsilon^2) = \varepsilon w_1 + \mathrm{O}(\varepsilon^2) \tag{17}$$

$$p = p_0 + \varepsilon p_1 + \varepsilon \frac{\partial p_0}{\partial z}\zeta_1 + \mathrm{O}(\varepsilon^2) = p_0 + \varepsilon p_1 + \mathrm{O}(\varepsilon^2) \tag{18}$$

$$\zeta = \zeta_0 + \varepsilon\zeta_1 + \mathrm{O}(\varepsilon^2) = \varepsilon\zeta_1 + \mathrm{O}(\varepsilon^2) \tag{19}$$

Here, u_0^+, w_0^+, p_0^+, v_0, w_0, p_0 are the base velocities and pressures of the upper layer and bottom layer.

After substituting the expansion into Eqs. (1)–(11) and collecting terms of order ε, the resulting two-dimensional disturbance equations are:

For the upper layer:

$$2\left(\frac{\partial u_0^+}{\partial z}\frac{\partial w_1^+}{\partial x}\right) = r^{-1}\left(-\frac{\partial^2 p_1^+}{\partial x^2} - \frac{\partial^2 p_1^+}{\partial z^2}\right) \tag{20}$$

$$\frac{\partial w_1^+}{\partial t} + u_0^+\frac{\partial w_1^+}{\partial x} = r^{-1}\left(-\frac{\partial p_1^+}{\partial z} + m\nabla^2 w_1^+\right) \tag{21}$$

For the bottom layer:

$$2\left(\frac{\partial u_0}{\partial z}\frac{\partial w_1}{\partial x}\right) = -\frac{\partial^2 p_1}{\partial x^2} - \frac{\partial^2 p_1}{\partial z^2} \tag{22}$$

$$\frac{\partial w_1}{\partial t} + u_0\frac{\partial w_1}{\partial x} = -\frac{\partial p_1}{\partial z} + \nabla^2 w_1 \tag{23}$$

For the boundary at the interface, $z = \zeta(x,t)$:

$$w_1^+ = \zeta_{1x} + u_0^+|_{z=0}\zeta_{1x} \tag{24}$$

$$w_1^+ - w_1 = 0 \tag{25}$$

$$-\frac{\partial w_1^+}{\partial z} + \frac{\partial w_1}{\partial z} + \left(\frac{\partial u_0^+}{\partial z} - \frac{\partial u_0}{\partial z}\right)\zeta_{1x} = 0 \tag{26}$$

$$m\left(\frac{\partial^2 w_1^+}{\partial z^2} - \frac{\partial^2 w_1^+}{\partial x^2}\right) = \frac{\partial^2 w_1}{\partial z^2} - \frac{\partial^2 w_1}{\partial x^2} \tag{27}$$

$$-p_1^+ + 2m\frac{\partial w_1^+}{\partial z} = -p_1 + 2\frac{\partial w_1}{\partial z} + G\zeta_1 - C\zeta_{1xx} \tag{28}$$

where

$$\zeta_{1x} = \frac{\partial \zeta_1}{\partial x}, \qquad \zeta_{1xx} = \frac{\partial^2 \zeta_1}{\partial x^2}$$

For the upper plate ($z = l$):

$$w_1^+ = \frac{\partial w_1^+}{\partial z} = 0 \tag{29}$$

For the lower plate ($z = -1$):

$$w_1 = \frac{\partial w_1}{\partial z} = 0 \tag{30}$$

We next use a normal mode expansion:

$$(w_1^+, p_1^+, w_1, p_1, \zeta_1)^t = [w^+(z), p^+(z), w(z), p(z), \zeta(z)]^t\, \mathrm{e}^{\mathrm{i}kx+\sigma t} \tag{31}$$

where k is the wavenumber and σ is the growth rate.

Eq. (31) was substituted into the governing equations (20)–(30), and a set of ordinary differential equations were then obtained for $w^+(z)$, $p^+(z)$, $w(z)$, and $p(z)$. Next, the linearized equations were converted into an eigenvalue problem where σ is the eigenvalue and the velocities and pressures are the eigenvectors. Finally, the eigenvalue problem was solved using a Chebyschev spectral tau method (Johnson, 1996; Canuto et al., 1998).

3. Experiment

The difficulty in achieving Couette flow in a straight channel comes from creating a constant bottom (or upper) wall motion, and from the set-up length of the base flow. In a previous paper (Barthelet et al., 1995), these difficulties have been overcome by bending a channel of rectangular cross-section into an annular ring. Our experiment closely follows their device (Fig. 2). The rotation of the bottom plate around the axis of the ring drags the fluids. However, owing to the radial velocity gradient and centrifugal forces, the velocity field may be distorted and further instabilities generated. We avoid these instabilities by maintaining slow rotation speeds (<0.29 rev/s). This arrangement has the following advantages: shearing is achieved by a rigid plate without any vibrations, flows are fully developed without any entry or discharge sections, and wave evolution can be observed over long periods of time. Compared with the experiments of Gallagher et al. (1996), we do not need to closely match the densities of the two fluids, and therefore, we can freely investigate the instability of different fluid combinations.

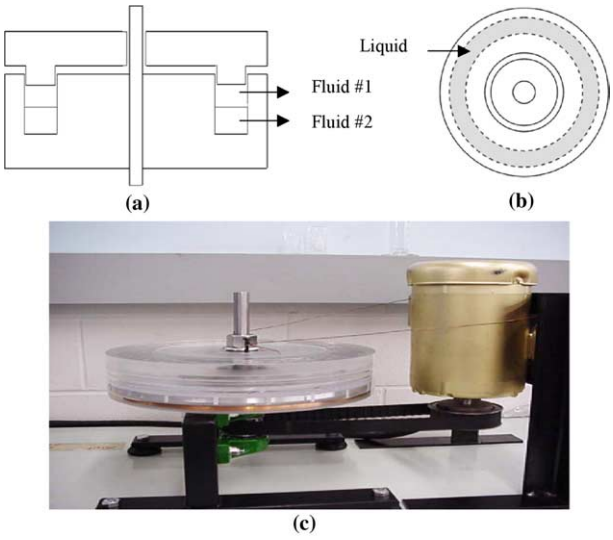

Fig. 2. Sketch and photo of the experimental device. (a) Side view, (b) top view, and (c) a picture of the experimental apparatus.

The channel is grooved in a PMMA plate, its mean diameter is 340 mm, the width is 50 mm, and the depth is 15 mm. The bottom plate is driven by a DC gearmotor (Dayton, model 6Z417A) through a gear chain. The speed can be adjusted with a DC speed controller. Air bubbles created during the filling of the channel are removed with a syringe through a small hole in the top plate.

To test the fluid instabilities at different physical properties, we used two silicone oils of different viscosities as the top fluids. The silicone oils were purchased from Clearco Products Co., their viscosities are 20cP, and 50cP and their densities are 0.946 and 0.955, respectively. The lower fluid was DI water.

The interfacial tensions between silicone oil and water were measured with a Kruss K12 processor tensiometer using a platinum–iridium DeNouy ring. The temperature of the fluids was kept constant at 30 ± 0.1 °C using a flow-through thermostat unit. The interfacial tension between water and 20cP silicone oil is 79.4 dyn/cm, it is 81.2 dyn/cm between water and 50cP silicone oil.

4. Results and discussion

4.1. Theoretical discussion

If there is no gravity stabilization, Yih's result (1967) shows that longwaves are always unstable if the depth ratio between the more viscous fluid and the thinner fluid is less than 2. Figs. 3 and 4 are the theoretical growth rate curves for the 50cP silicone oil/water system and 20cP silicone oil/water system, respectively. For the 50cP silicone oil/water system, Fig. 3 shows that at low Reynolds numbers the slope of the growth rate at zero wavenumber is negative. When the Reynolds number reaches about 1200, the slope of the growth rate at zero wavenumber becomes positive, which means that the long-wavelengths become unstable. The story is similar for the 20cP silicone oil/water system. Fig. 4 shows that when the Reynolds number reaches about 1900, the slope of the growth rate at zero wavenumber switches from negative to positive and the longwave region becomes unstable.

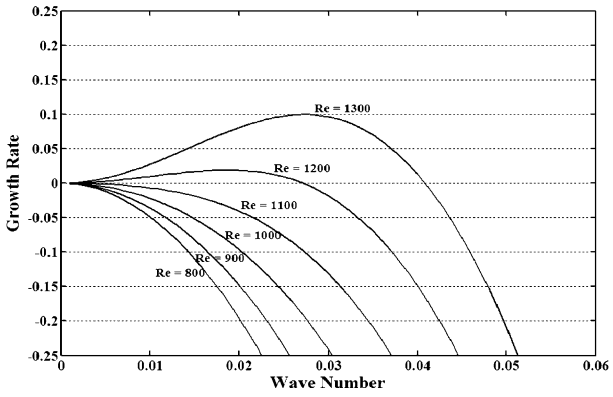

Fig. 3. Growth rate curves for the 50cP silicone oil/water system at different Reynolds numbers when the depth ratio is 1. This figure shows that when the Reynolds number is less than 1100, the flow is stable to longwaves. When the Reynolds number is greater than 1200, the flow becomes unstable to longwaves.

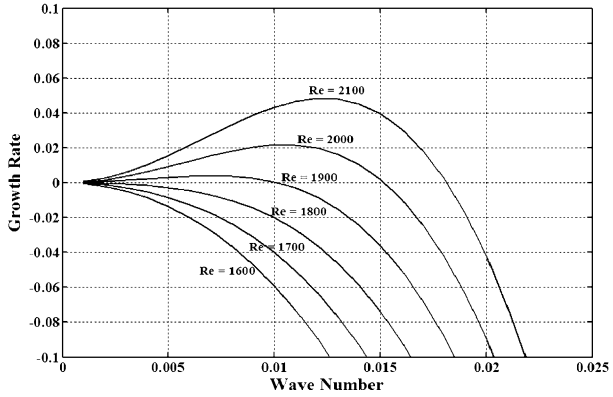

Fig. 4. Growth rate curves for the 20cP silicone oil/water system at different Reynolds numbers when the depth ratio is 1. This figure shows that when the Reynolds number is less than 1800, the flow is stable to longwaves. When the Reynolds number is greater than 1900, the flow becomes unstable to longwaves.

As in reference of Gallagher et al. (1996), our linear instability analysis shows that the interfacial instability regime depends strongly on the depth ratio. Fig. 5 shows the growth rate curves for the 50cP silicone oil/water system at different depth ratios when the Reynolds number is 1800 (a typical number in our experimental set-up). It shows that when the depth ratio is less than 1, the growth rate curves have a positive slope at 0 wavenumber at a finite Reynolds number and the flow is in

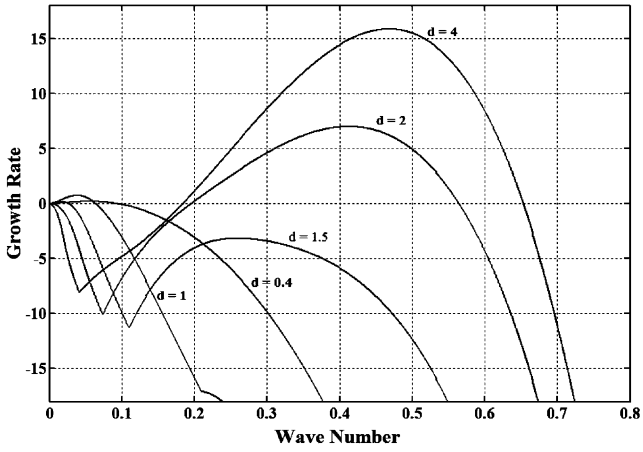

Fig. 5. Growth rate curves for that 50cP silicone oil/water system at different depth ratios when the Reynolds number is 1800. This figure shows that when the depth ratio is less than 1, the longwave is unstable, when the depth ratio is larger than 2, the flow is unstable to shortwaves.

the longwave unstable regime. However, when the depth ratio is more than 2, the growth curves always have a negative slope at 0 wavenumber; therefore, the flow is stable to longwaves, which is called the "thin-layer" effect (Hooper and Boyd, 1987; Renardy, 1987). In this region, the flow is unstable to shortwaves. Fig. 5 shows that when the depth ratio is 3 and 4, the wavenumber of this shortwave instability is around 0.45. It is important to mention that when the depth ratio is 1.5, both longwave instability and shortwave instability exist.

4.2. Comparison between experimental and theoretical results

In our experiments, we rotate the bottom plate and slowly increase the speed until waves are seen at the interface. We recorded the critical rotation speed, calculated the critical experimental Reynolds number, and compared it with the critical theoretical Reynolds number. The following formula was used to calculate the critical Reynolds number.

$$Re = \frac{dU_0\rho}{\mu} \tag{32}$$

In the shortwave instability regime,our experimental data show good agreement with the theoretical data. Figs. 6 and 7 are the comparison between the critical experimental Reynolds number and the critical theoretical data for the 50cP silicone oil/water system and 20cP silicone oil/water system, respectively. Both figures show that the difference between the experimental data and the theoretical data are within the tolerance of the experiment. Therefore, the linear instability analysis can predict quantitatively the onset of the two-layer fluid flow instability in the shortwave instability regime. All of the waves in our experiments have a regular and steady wavelength.

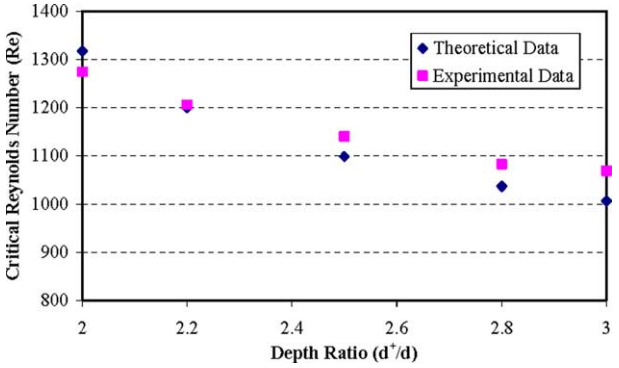

Fig. 6. Experimental and theoretical critical Reynolds number for the 50cP silicone oil/water system at different depth ratios when flow is in the shortwave instability regime. This figure shows that the theoretical results of the linear instability analysis agree well with the experimental results at these conditions.

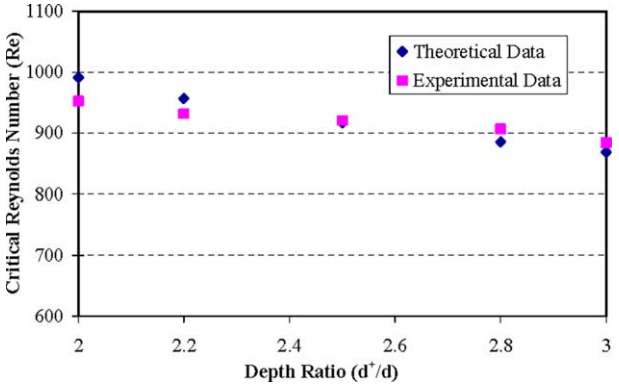

Fig. 7. Experimental and theoretical critical Reynolds number for the 20cP silicone oil/water system at different depth ratios when flow is in the shortwave instability regime. This figure also shows that the theoretical results of linear instability agree well with the experimental results for the 20cP silicone oil/water system in the shortwave instability regime.

The story is different, however, in the longwave instability regime. As previously discussed, linear instability analysis predicts that when the depth ratio is smaller than 2, the flow is stable to the shortwave instability. In our experiments, the shortwave instabilities were found in all depth ratios even when the depth ratio is less than 1. Fig. 8 is a photo of the waves for the 50cP silicone oil/water system when the depth ratio is 0.75. As was the case in the shortwave regime, the waves found in this regime also have a regular wavelength and once the waves occur, they are stable at constant rotation speeds. If we further increase the rotation speed, the amplitude of the waves increases and the wavelength of the waves decreases until the rotation speed is so high that mixing of the two fluids occur.

Fig. 9 is the critical experimental Reynolds number for the 50cP silicone oil/water system when the depth ratio is less than 1. Fig. 9 shows the same trend as the

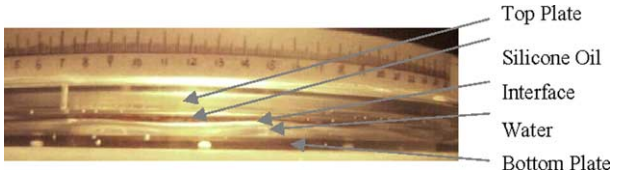

Fig. 8. Photo of the short-wavelength instability (50cP silicone oil/water, $l = 0.75$).

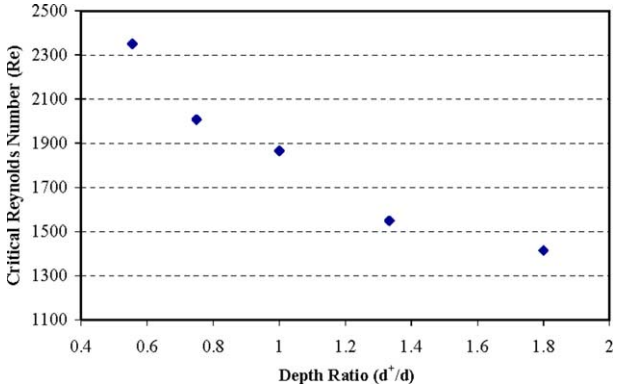

Fig. 9. Experimental critical Reynolds number for the 50cP silicone oil/water system, when the depth ratio is less than 2. At this region, linear instability analysis predicts no shortwave instability, however, instabilities are still seen in the experiments ($Re = dU_0\mu/\rho$ is based on the bottom layer).

experimental data in Figs. 6 and 7. Due to the gravitational stabilization, there is a critical Reynolds number, above which the instability occurs and the critical Reynolds number decreases with an increase of the depth ratio. Moreover, the absolute value of the critical Reynolds numbers in Fig. 9 is not significantly different from that in Figs. 6 and 7. Fig. 10 is the critical wavenumber and wavelength of the system for different depth ratios. The wavelength is from 7.1 to 4.7 cm and decreases with an increase in the depth ratio.

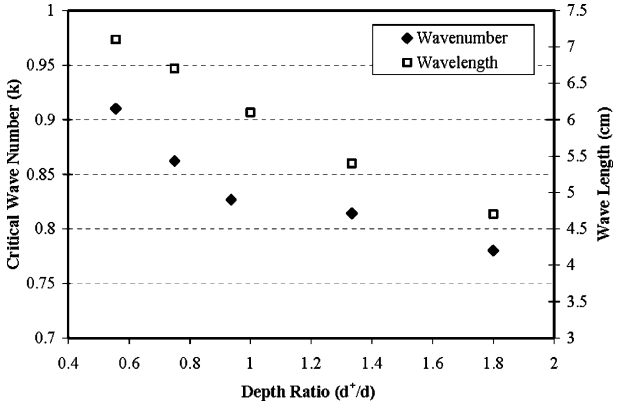

Fig. 10. Experimental critical wavenumber and wavelength for the 50cP silicone oil/water system, when the depth ratio is less than 2. Both the critical wavenumber and wavelength decrease with an increase in depth ratio.

We believe there are two possible reasons for this disagreement. The first reason is due to the dimensional limitation of the experimental apparatus. Fig. 3 shows that the wavenumber of the fastest growing longwave is usually between 0.02 and 0.03 for 50cP silicone oil/water system when the depth ratio is 1. The dimensionless wavenumber, k is defined by

$$k = 2\pi\frac{d}{\lambda} \tag{33}$$

where d is the thickness of the bottom, λ is the wavelength. When the wavenumber is 0.03, the wavelength is about 1500 cm. However, the length of the channel in our experiment is about 210 cm, which is much shorter than the wavelength of the longwaves. Therefore, the dimensional limitation of the experiments will resist the development of the longwaves. The second reason for this is probably because our experimental system is a three dimensional channel flow instead of a two dimensional plane flow, the existence of the outside and inside walls will also resist the development of the longwaves and causes the development of the shortwaves.

4.3. The theoretical prediction of the influence of the fluid property ratios on the onset of the shortwave instability

From the previous discussion, we see that the linear instability analysis method can predict the onset of the shortwave instability, this section of the paper studies the influence of the viscosity ratio, density ratio, and depth ratio on the shortwave instability of the two-layer flow using the linear instability analysis method.

4.3.1. The influence of viscosity ratio on the stability

Figs. 11 and 12 are the critical Reynolds numbers at various viscosity ratios when we change the viscosity of the upper layer and bottom layer, respectively. Fig. 11 shows that with an increase in the viscosity ratio (i.e. an increase of the viscosity in the upper layer), the critical Reynolds number increases. This means that the critical velocity increases and the fluid becomes more stable. Therefore, the increase of the viscosity of the upper layer is beneficial to the stability of the fluid.

Because our critical Reynolds number is $Re = dU_0\mu/\rho$, the change in the viscosity of the bottom layer causes a change in the critical Reynolds number even when the critical velocity does not change. Therefore, for the problem where the viscosity of the bottom layer changes, the critical Reynolds number defined in this way cannot represent the stability of the fluid. For this problem, we can define the critical Reynolds number $Re^+ = d^+U_0\mu^+/\rho^+$, because d^+, ρ^+ and μ^+ are constant in this problem. Fig. 12 shows the change in the critical Reynolds number, Re^+, with the change in the viscosity ratio when the viscosity of the bottom layer decreases.

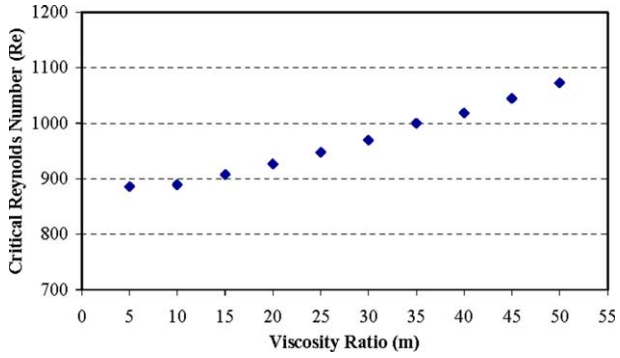

Fig. 11. The critical Reynolds number, Re, at various viscosity ratios when the viscosity of the upper layer fluid increases ($Re = dU_0\mu/\rho$, $r = 0.95$, $l = 3$, $\rho = 1000$ kg/m^3, $G = 2000$ and $C = 350,000$). When the viscosity of the upper fluid increases, the critical Reynolds number increases and the flow becomes more stable.

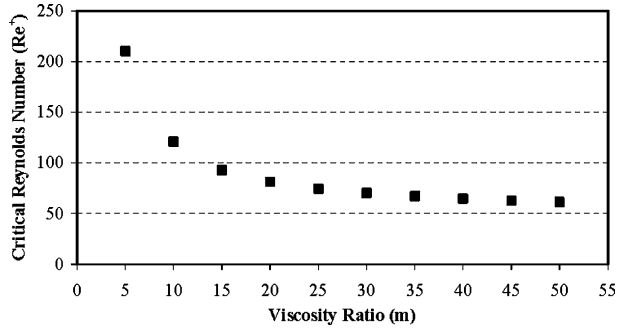

Fig. 12. The theoretical critical Reynolds number, Re^+, at various viscosity ratios when the viscosity of the bottom layer decreases ($Re^+ = d^+U_0^+\mu^+/\rho^+$, $r = 0.95$, $l = 3$, $\rho = 1000$ kg/m^3, $G = 0.8$ m^2 and $C = 140$ m^2). When the viscosity of the bottom fluid decreases, the fluid becomes more unstable. Therefore, an increase in the viscosity of the bottom fluid makes the flow more stable.

In Fig. 12, Re^+ decreases when the bottom layer viscosity decreases. The critical velocity also decreases and the fluid becomes more unstable. Therefore, a decrease in the viscosity of the bottom layer causes the fluid to become more unstable and an increase in the viscosity of the bottom layer is beneficial to the stability of the fluid. This is the same result as before when the top layer viscosity increased.

4.3.2. The influence of the density ratio on the stability

Figs. 13 and 14 give the change of the critical Reynolds number with a change of the density ratio when the densities of the upper layer and bottom layer change, respectively. From Fig. 13, we see that with an increase in the density ratio by increasing the density of the upper layer decreases the critical Reynolds number. This means that the critical velocity decreases and the fluid becomes more unstable. Therefore, decreasing the density of the upper layer is beneficial to the stability of the fluid. This is easy to understand because of the gravitational stabilization.

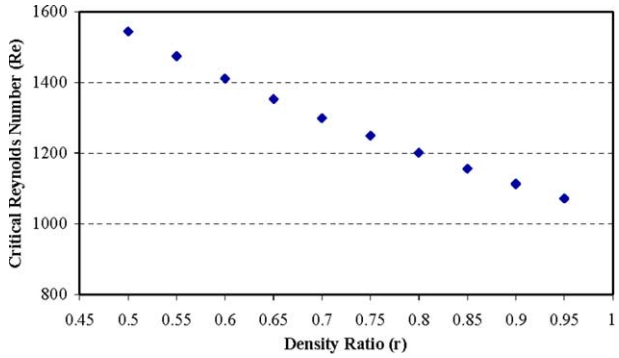

Fig. 13. The theoretical critical Reynolds number, Re, at various density ratios when the density of the upper layer increases ($Re = dU_0\mu/\rho$, $l = 3$, $\rho = 1000$ kg/m^3, $m = 50$, $G = 40,000(1 - r)$ and $C = 350,000$). When the density of the upper fluid increases, the critical Reynolds number decreases and the flow becomes more unstable.

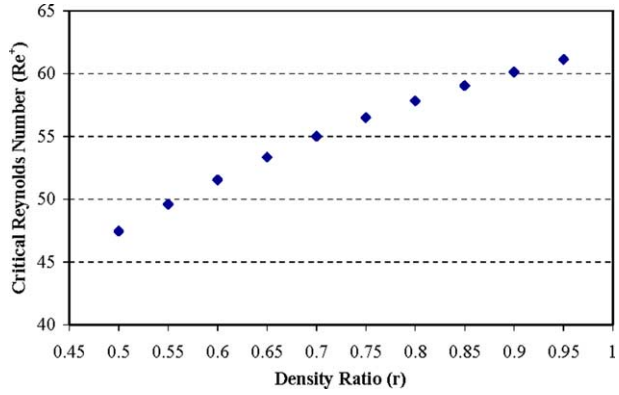

Fig. 14. The theoretical critical Reynolds number, Re^+, at various density ratios when the density of the bottom layer decreases ($Re^+ = d^+U_0\mu^+/\rho^+$, $m = 50$, $l = 3$, $\rho^+ = 950$ kg/m^3, $G = 40,000$ $(1 - r)/r$ and $C = 350,000$). A decrease in the density of the bottom fluid increases the critical Reynolds number and the flow becomes more unstable.

When the viscosity of the bottom layer changes, we have the same problem as before, where the Reynolds number must be defined in terms of the upper layer parameters. For this problem, we use the critical Reynolds number $Re^+ = d^+U_0\mu^+/\rho$. Fig. 14 shows the change of the critical Reynolds number, Re^+, at various density ratios ratio when the viscosity of the bottom layer decreases.

In Fig. 14, when the density ratio increases by decreasing the density of the bottom layer, the critical Reynolds number, Re^+, increases. This indicates that the critical velocity increases and the flow becomes more stable. Therefore, decreasing the density of the bottom layer is beneficial to the stability of the fluid. The reason for this is probably when the density of the bottom layer increases, more energy is put into the system for the same rotation speed.

5. Summary and conclusion

Linear instability analysis shows that depending on the depth ratio, the interfacial instability of two-layer fluid flow can be a longwave or a shortwave instability, respectively. In this paper, we compared our experimental results with the theoretical results of a linear instability analysis. The results show that in the shortwave regime, the experimental result agrees well with the theoretical prediction of the linear stability analysis. However, we find shortwaves in our experiment even in the range of depth ratios where the linear instability analysis predicts only the longwaves are unstable. The reasons for this are believed to be the finite length of the channel and the influence of the inside and outside wall in our experiments.

In this paper, we also investigated the influence of the viscosity and density of the fluid on the onset of the shortwave instability using linear instability analysis. The result shows that increasing the viscosity of both layers makes the system more stable and decreasing the density of both layers makes the system more stable.

Acknowledgements

The authors would like to thank the Alabama Department of Economic and Community Affairs and the University of Alabama MINT Center for their support.

References

Barthelet, P., Charru, F., Fabre, J., 1995. Experimental study of interfacial long waves in a two-layer shear flow. J. Fluid Mech. 303, 23–53.

Canuto, C., Hussaini, M.Y., Quarteroni, A., Zhang, T.A., 1998. Spectral Methods in Fluid Dynamics. Springer-Verlag, Berlin.

Gallagher, G.T., Leighton, D.T., McCready, M.J., 1996. Experimental investigation of a two layer shearing instability in a cylindrical Couette cell. Phys. Fluid 8, 2385–2392.

Hooper, A.P., Boyd, W.G.C., 1983. Shear flow instability at the interface between two viscous fluids. J. Fluid Mech. 128, 507–528.

Hooper, A.P., Boyd, W.G.C., 1987. Shear flow instability at the interface between two viscous fluids. J. Fluid Mech. 179, 201–225.

Johnson, D., 1996. Chebyshev polynomials in the spectral tau method and application to eigenvalue problems. NASA Technical Report #CR-198451.

Kao, T.W., Park, C., 1972. Experimental investigations of the stability of channel flows, Part 2: Two layered co-current flow in a rectangular channel. J. Fluid Mech. 52, 401–410.

Kuru, W.C., Sangalli, M., Uphold, D.D., McCready, M.J., 1985. Linear stability of stratified channel flow. Int. J. Multiphase Flow 21, 733–753.

Renardy, Y., 1985. Instability at the interface between two shearing fluids in a channel. Phys. Fluids 28, 3441–3443.

Renardy, Y., 1987. The thin-layer effect and interfacial stability in a two-layer Couette flow with similar liquids. Phys. Fluids 30, 1627–1637.

Sangalli, M., Gallagher, C.T., Leighton, D.T., Chang, H.C., McCready, M.J., 1995. Finite-amplitude waves at the interface between fluids with different viscosity: theory and experiments. Phys. Rev. Lett. 75, 77–80.

Yih, C.S., 1967. Instability due to viscosity stratification. J. Fluid Mech. 27, 337–352.